Progress In Electromagnetics Research, Vol. 166, 107–117, 2019

Two-Photon Luminescence and Second Harmonic Generation of Single Layer Molybdenum Disulphide Nanoprobe for Nonbleaching and Nonblinking Optical Bioimaging

Qiuqiang Zhan[1, #], Xin Zhang[1, #], Baoju Wang[1], Nana Li[1], and Sailing He[1, 2, 3, *]

Abstract—Layered molybdenum disulphide (MoS_2) can efficiently emit photoluminescence (PL) excited by visible light. However, one-photon PL of MoS_2 for bioimaging purposes suffers from strong autofluorescence and ion-induced PL quenching. Herein, we report single layer chitosan decorated MoS_2 nanosheets as nonbleaching and nonblinking optical nanoprobes under near infrared femtosecond laser excitation and their applications for two photon luminescence (TPL) and second harmonic generation (SHG) bioimaging. The TPL can resist the ion-induced quenching by the cellular membrane. The proposed TPL and SHG of single layer MoS_2 show great potential for real-time, deep and multiphoton bioimaging.

1. INTRODUCTION

Layered two-dimensional nanomaterials have attracted much attention since the birth of graphene isolated from graphite [1]. Beyond graphene, transition-metal dichalcogenides (TMDs) have been highly studied because of their rich electronic, optical, mechanical and chemical properties as well as promising applications in sensing, catalysis, energy storage and biomedicine [2–5]. Molybdenum disulphide (MoS_2), containing of one plane of molybdenum atoms sandwiched between two planes of sulfur atoms, is a primary focused TMD [6–8]. Because of the relatively weak Van der Waals forces between their layers and the strong intralayer interactions, the exfoliation of single layer MoS_2 from its bulk counterpart was realized [9]. Unlike the bulk materials, single layer MoS_2 nanosheets (SLMNs) are a direct band gap semiconductor material, making them emit strong photoluminescence (PL) [10, 11]. The one-photon excited luminescence from layered MoS_2 nanosheets has already been applied to biosensing and bioimaging research (although the PL of multilayer MoS_2 is relatively quite weak) [12, 13].

However, the ultraviolet-visible light excited one-photon luminescence bioimaging applications has some drawbacks, such as strong autofluorescence and the very limited imaging depth due to the strong scattering of short-wavelength photons [14]. Nonlinear optical imaging using near infrared (NIR) light can avoid those drawbacks. Nonlinear optical imaging (e.g., two-photon luminescence (TPL) and second harmonic generation (SHG) imaging) using the excitation wavelength in the first NIR window (650–900 nm) or the second NIR window (1000–1300 nm) has many advantages, such as low autofluorescence, reduced photobleaching and the remarkable capability for deep tissue imaging [15–17]. Although the extinction coefficient of SLMNs is larger than those of graphene oxide and gold nanorods under the NIR [18, 19], the one photon excited PL is hard to be detected at the long (e.g., 600 nm) excitation wavelength. Recently, an exceedingly large two-photon absorption coefficient (larger than that of

Received 25 July 2019, Accepted 20 December 2019, Scheduled 23 December 2019

* Corresponding author: Sailing He (sailing@zju.edu.cn).

[1] Centre for Optical and Electromagnetic Research, South China Academy of Advanced Optoelectronics, South China Normal University, Guangzhou 510006, P. R. China. [2] Centre for Optical and Electromagnetic Research, National Engineering Research Center for Optical Instruments, Zhejiang University, Hangzhou 310058, P. R. China. [3] Department of Electromagnetic Engineering, Royal Institute of Technology, Stockholm 10054, Sweden. # These authors equally contribute to this work.

conventional semiconductors by three orders of magnitude) and a large laser damage threshold of single layer MoS_2 island were reported [20]. SHG and third harmonic generation from single or few layers MoS_2 film were also reported [21–23]. MoS_2 nanosheets are expected to be NIR-excited optical nanoprobes for bioimaging. However, we are hardly aware of research on the TPL and SHG properties of small size (sub-100 nm) SLMNs and their application in bioimaging.

In this work, we reported the strong and stable TPL and SHG from small chitosan (CS) decorated SLMNs (CS-MoS_2 nanosheets) with sub-100 nm lateral dimension. Excited by the first NIR window light, CS-MoS_2 nanosheets show strong TPL with its peak at 525 nm at a low power of 3 mW. Under the excitation of the second NIR window, strong SHG with sharp peaks were observed at a lower power of 1 mW. In addition, the TPL and SHG from CS-MoS_2 nanosheets were demonstrated to be nonbleaching and nonblinking. As a result, CS-MoS_2 nanosheets were carried out to TPL and SHG imaging and cellular three-dimensional (3D) scanning imaging under low power laser excitation. Furthermore, the reported quenching of TPL from MoS_2 nanosheets on the cellular membrane was not observed, indicating their feasibility in bioimaging.

2. EXPERIMENTAL

2.1. Materials

N,N-Dimethylformamide (DMF), acetone, methanol and acetic acid were purchased from Sino Chemical Reagent Co., Ltd. Ionic liquid (IL) 1-butyl-3-methylimidazolium hexafluorophosphate (BMIPF6) ($\geq$ 97.0%) and chitosan (CS) were purchased from Aladdin Reagent. Molybdenum sulfide (MoS_2) with a bulk particle size $< 2\,\mu m$ were purchased from Sigma-Aldrich. Cell Counting Kit-8 (CCK-8, 99.9%) was purchased from Beyotime Biotechnology. Dulbecco's modified eagle medium (DMEM, 99%), phosphate buffered saline (PBS), and fetal bovine serum (FBS, 99%) were purchased from Gioco Life technology. All chemical reagents were used without further purification, and deionized water was used in all the experimental procedures.

2.2. IL-Assisted Exfoliation of Single Layer CS-MoS_2 Nanosheets

The preparation of CS-MoS_2 nanosheets was done according to Zhang's method with some modifications [24]. 250 mg of bulk MoS_2 powders and 0.5 mL of IL were added to the mortar and ground forcibly for 90 minutes. Then 100 mg of CS was then added into the mortar, followed by grinding for another 30 minutes. The collected mixture was added into a solution of DMF and acetone (DMF : acetone = 1 : 1, v/v) and centrifuged at 12000 rpm for 20 minutes. In order to remove the excess CS, the mixture was added into acetic acid solution (acetic acid : water = 0.5%, v/v) and centrifuged at 12000 rpm for 20 minutes. The entire washing cycle was repeated twice. The collected precipitant was re-dispersed into deionized water and further centrifuged at 2000 rpm for 45 min, twice. The supernatant containing CS-MoS_2 nanosheets was diluted with water to 5 mL for the following investigations. The resulting concentration of CS-MoS_2 nanosheets in water was calculated to be 1.15 mg/mL by drying the supernatant. The MoS_2 nanosheets and CS-MoS_2 nanosheets utilized the same purification method.

2.3. Characterization

Transmission electron microscope (TEM) images were obtained with a JEM-2100HR transmission electron microscope (JEOL). Atomic force microscopy (AFM) images were obtained with a Bruker Multimode 8 atomic force microscope. The absorption spectra of the CS-MoS_2 nanosheets in deionized water were acquired with a Lambda 950 UV-vis-NIR spectrophotometer (PerkinElmer). Photoluminescence spectra and images of CS-MoS_2 nanosheets were recorded using a home-built optical measurement system.

2.4. Optical Measurement System

The optical measurement system was based on an inverted multi-photon scanning microscope (IX81, Olympus), a tunable Ti: Sapphire laser as the excitation source (Coherent Mira HP, 76 MHz femtosecond

pulse mode at 750–920 nm), an optical parameter oscillator (Synchronized Coherent Mira OPO, 76 MHz femtosecond plus mode 1000–1600 nm), and a fibre spectrometer (QE65Pro, Ocean Optics). The excitation beam from the Mira HP or Mira OPO passed through a polarizing beamsplitter cube (PBS, Thorlabs) and a galvanometer system. After being reflected by a 670-nm dichroic mirror (Semrock) or 950-nm dichroic mirror (Chroma) and directed into the oil immersion objective (60×, NA = 1.35, Olympus), the excitation laser beam was focused on the sample. The luminescence signal from the sample was backward captured by the same objective. A band-pass filter (FF01-525/30-25 or FF01-550/49-25, Semrock) was used to further block the excitation light between objective and reflection mirrors. The fluorescence light was directed into a PMT to obtain fluorescence images (Excitation power: 0–5 mW). In addition, without silver mirror (M5), the fluorescence light was collected by a fluorescence spectrometer for spectral analysis.

2.5. Cytotoxicity of CS-MoS_2 Nanosheets

HeLa cells (6 × 103) in 100 µL of DMEM medium (10% FBS, 100 U/mL penicillin, 100 µg/mL streptomycin) were seeded onto 96-well plates for 24 hours. The cells were then incubated with different concentrations of CS-MoS_2 nanosheets for 12 hours. To remove the redundant nanosheets, the cells were washed by PBS twice and cultured in a flash medium for another 24 hours. Afterward, 10 µL of the CCK-8 solution were added to each well, followed by incubation for another 1 hour. Cell viability was determined by measuring the absorbance at the wavelength of 450 nm with a microplate reader. All measurements were conducted in triplicate.

2.6. Bioimaging of CS-MoS_2

Hela cells were seeded onto the confocal dish and grown in 1.5 mL of complete medium (DMEM medium, 10% FBS, 100 U/mL penicillin, 100 µg/mL streptomycin) at 37°. After 24 hours, the cells were incubated with CS-MoS_2 nanosheets for 12 hours. The excess nanosheets were then washed by PBS, twice. The cells were observed via scanning microscopy with a 60× oil immersion objective lens with excitation at 750 nm and 1050 nm.

3. RESULTS AND DISCUSSION

SLMNs were exfoliated from bulk MoS_2 powders and then transferred to become soluble according to previously reported method with some modifications [24]. The atomic force microscopy (AFM) image (Figure 1(a)) shows that the thickness of the exfoliated MoS_2 nanosheets is 0.7–1 nm, indicating the single layer structure (0.65 nm in theory) [25]. To improve the chemical stability and biocompatibility, SLMNs were decorated with CS [26]. The presence of CS in the CS-MoS_2 nanosheets is characterized by the results of Fourier transform infrared spectra (Figure 1(b)). The size of the CS-MoS_2 nanosheets were determined to be below 100 nm (Figure 1(c)). Compared to SLMNs, the thickness of CS-MoS_2 nanosheets increase to $\sim$ 1.5 nm due to the attachment of CS. The formation of single-layered structures of CS-MoS_2 nanosheets was also confirmed by the observation of no multi-steps on the edges (Figure 1(d), the multi-layer CS-MoS_2 nanosheets were obtained from the precipitant of the final process.) [27]. Raman spectra of CS-MoS_2 nanosheets were measured to give bands at 384 cm^1 (the in-plane vibration E^1_{2g} mode of 2H-MoS_2 crystal) and 407 cm^1 (the out-of-plane vibration A_{1g} mode of 2H-MoS_2 crystal), respectively (Figure 1(e)) [28]. Being exfoliated from bulk powders, the wavenumber difference of CS-MoS_2 nanosheets between the two peaks decreases from 25.5 to 22.5 cm^{-1} as the number of layers decreases because of the anomalous lattice vibration [29]. It is worth mentioning that the liquid-phase exfoliated single layer nanosheets showed a different position from the mechanically exfoliated single layer nanosheets due to surface adsorption [9].

CS-MoS_2 nanosheets show four characteristic optical absorption bands with peaks at 400 nm, 447 nm, 606 nm and 667 nm, in good agreement with the observation of the liquid exfoliated SLMNs (Figure 2(a)) [9]. The relatively weak optical absorption bands at 606 nm and 667 nm and the strong absorption peaks at 400 nm and 447 nm suggest the existence of a large number of small sized nanosheets due to the quantum size effect [30]. In general, layered MoS_2 with large size shows two down-converted

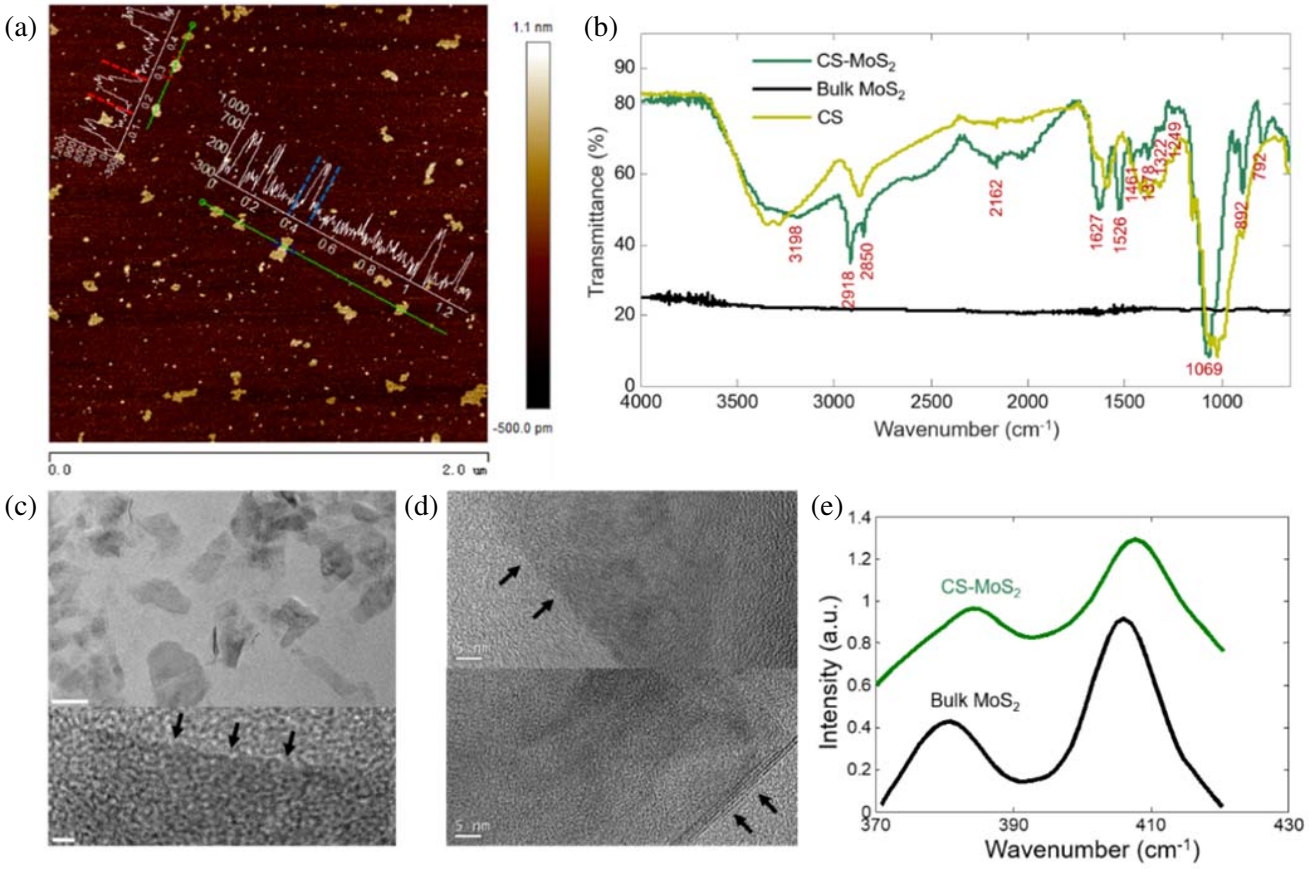

Figure 1. (a) AFM image of SLMNs. Insert: Thickness profile of SLMNs along with green lines. The unit of values on the vertical axis are picometers. (b) Fourier transform infrared spectra for CS, bulk MoS_2 and CS-MoS_2 nanosheets. (c) Upper: TEM image of CS-MoS_2 nanosheets. The scale bar: 50 nm. Bottom: High-resolution TEM image at an edge (indicated by black arrows) of a CS-MoS_2 nanosheet. The scale bar: 2 nm. (d) TEM images of CS-MoS_2 nanosheets at edges. Upper: single layer CS-MoS_2 nanosheets. Bottom: 4–5 layers CS-MoS_2 nanosheets. The scale bar: 5 nm. (e) Raman spectra of bulk MoS_2 and CS-MoS_2 nanosheets. It should be noted that there is no obvious Raman peaks from chitosan due to richness of functional groups such as -CH_2, -COOH, -NH_2, whose Raman peaks are mainly located between 1000 and 4000 cm^{-1}.

PL peaks at around 627 nm and 670 nm when excited by continuous visible light [31]. When the lateral dimension of the layered MoS_2 decreases to 100 nm or smaller, these two peaks are sharply weakened and another new blue-shifted PL band appears. The new peak is excitation-wavelength dependent and can be attributed to the blue-shifted hot PL from the K point [12, 32]. This phenomenon would induce cross-talk among emission detection channels in fluorescent microscopic imaging. In addition, the emission of the two peaks cannot be observed at the long (e.g., 600 nm) excitation wavelength [32]. Short wavelength excitation would impose the problems of strong autofluorescence in bio-samples as well as the resulting limited imaging depth. Therefore, one photon excited PL of layered MoS_2 nanosheets is not suitable for bioimaging applications. In contrast, nonlinear optical imaging is more suitable for bioimaging. Herein, the femtosecond (fs) laser was used to give a comprehensive view of the TPL and SHG properties of CS-MoS_2 nanosheets. As shown in Figure 2(b), excited by the laser of 750–920 nm, the PL peak of CS-MoS_2 nanosheets is unvarying and centered at 525 nm. A 1.94 order of excitation power dependence of PL was obtained (Figure 2(c)), indicating that the PL is due to two-photon excitation. Interestingly, unlike one photon excited luminescence, the TPL spectra of the layered MoS_2 nanosheets were not found to be excitation-wavelength dependent. This allows great flexibility in choosing the light source. Since

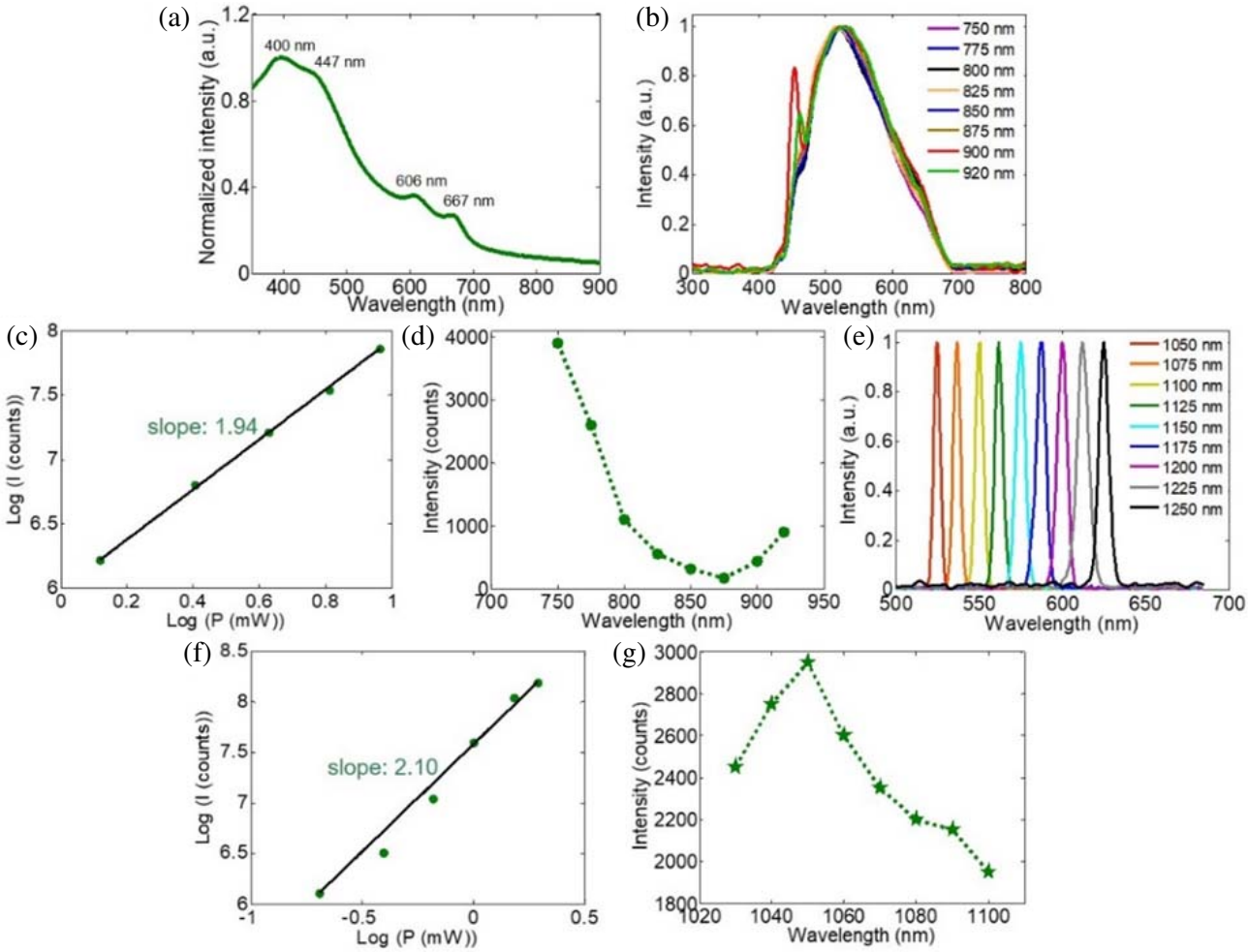

Figure 2. (a) Absorption spectra of CS-MoS_2 nanosheets. (b) TPL spectra of CS-MoS_2 nanosheets excited by a range of wavelengths from 750 nm to 920 nm. (c) A logarithmic plot of the TPL intensity as a function of excitation power. (d) Related TPL intensity of CS-MoS_2 nanosheets under the different excitation wavelengths with the same power. (e) SHG spectra of CS-MoS_2 nanosheets excited by a range of wavelengths from 1050 nm to 1250 nm using micro-spectroscopy. The spectral resolution is about 1 nm. (f) A logarithmic plot of the SHG intensity as a function of excitation power. (g) Related SHG intensity of CS-MoS_2 nanosheets under the different excitation wavelengths with the same power.

the emission wavelength of the one photon excited PL is a function of the lateral dimension of MoS_2 nanosheets, we speculate that this phenomenon may result from the relatively even distribution of their lateral dimensions [12]. When varying the excitation wavelength at the same power (3 mW), 750 nm light exerts the best excitation efficiency (Figure 2(d)). Interestingly, two additional sharp peaks were observed when CS-MoS_2 nanosheets are excited by 900 nm and 920 nm light. According to the frequency relationship between the incident light and the emergent light peak in the spectra, they are potentially attributable to the SHG. These signals have not been detected under the excitation of 750–875 nm, probably because the intensity of TPL is much larger than that of SHG as well as the limitations of the optical detection system setup. This phenomenon also appeared when excited by the wavelength at the second NIR optical window. The spectral profiles of CS-MoS_2 nanosheets were observed clearly when CS-MoS_2 nanosheets were excited by 1050–1250 nm light, as shown in Figure 2(e). A 2.1 order of excitation power dependence of luminescence was obtained (Figure 2(f)), in good agreement with the second order nonlinearity of the SHG process. Under the illumination of different wavelength (1030–1100 nm) with the same power (1 mW), 1050 nm light shows the greatest efficiency (Figure 2(g)). No

TPL were observed under the excitation of 1030–1250 nm, probably due to the wavelength dependent TPL efficiencies. The CS-MoS_2 nanosheets showed strong nonlinear optical signals under the excitation of both the first and second NIR windows with low power, indicating their great potential for optical bioimaging applications.

Most organic dyes suffer from serious photobleaching effects. Semiconductor Quantum dots have very high emission efficiency and have no photobleaching, but rather suffer from photoblinking [33]. These are not beneficial to optical bioimaging, and it is necessary to develop optical nanoprobes possessing greater photostability properties. The photostability properties of TPL and SHG of CS-MoS_2 nanosheets were explored under continuous fs laser exposure for an extended time. The TPL intensity of CS-MoS_2 nanosheets have hardly any change under continuous fs laser exposure for an extended time of 600 seconds (Figure 3(a)), suggesting they do not suffer from photobleaching. To further explore whether the nonlinear optical signals of CS-MoS_2 nanosheets possess nonbleaching or nonblinking properties, the time traces of TPL and SHG intensities were obtained under continuous fs laser illumination. No TPL fluctuation is observed after 10 minutes of continuous scanning with 200 μs temporal resolution (Figure 3(b)). The intensities of TPL coincide with a Gaussian distribution function (Figure 3(c)), indicating that CS-MoS_2 nanosheets are completely nonphotobleaching [34, 35]. Increasing the temporal resolution to 2 μs, the nonphotoblinking property of CS-MoS_2 nanosheets was also demonstrated (Figures 3(d) and 3(e)) [36]. Using the same procedure, the nonbleaching and nonblinking properties of SHG from CS-MoS_2 nanosheets were also demonstrated. The absence of photobleaching and photoblinking effects, combined with the high brightness under NIR excitation, make CS-MoS_2 nanosheets a new type of optical probes for efficient imaging.

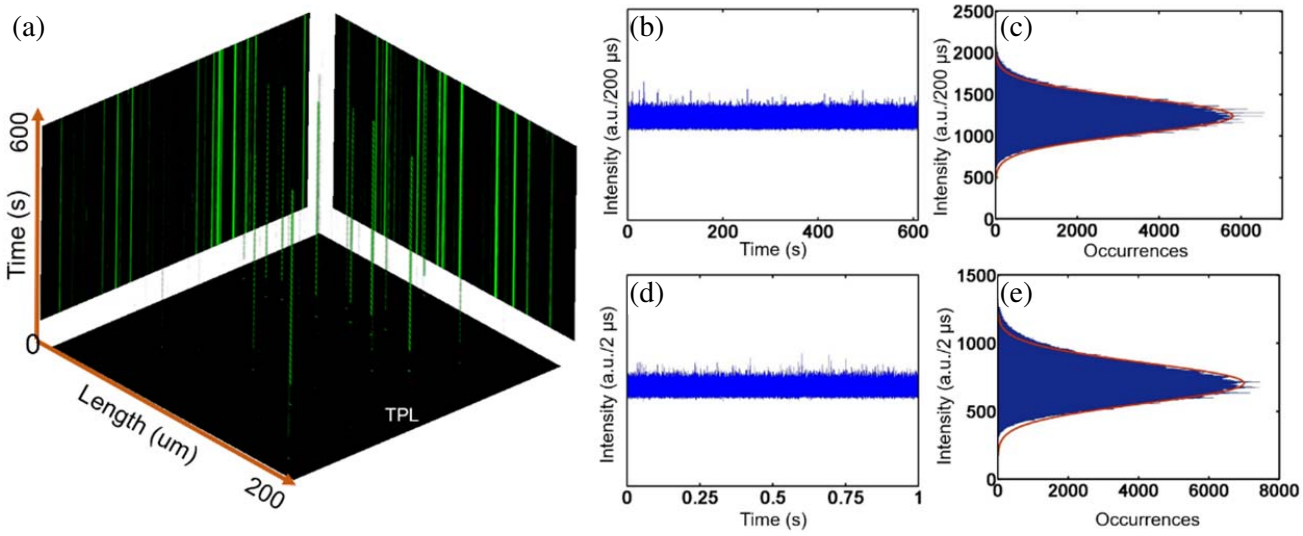

Figure 3. Photostability of TPL from CS-MoS_2 nanosheets. (a) Time trace repeated scanning image under continuous fs laser exposure for an extended time of 600 seconds. The pixel dwell time was 8 μs. (b) The time trace of TPL intensity from a single light-emit spot under continuous fs laser illumination for 10 minutes with 200 μs temporal resolution. (c) A histogram of TPL intensity of Figure 3(b) fitted with a Gaussian distribution function. (d) The time trace of TPL intensity from a single light-emit spot under continuous fs laser illumination for one second with 2 μs temporal resolution. (e) A histogram of TPL intensity of Figure 3(d) fitted with a Gaussian distribution function.

Based on the above results, water-soluble CS-MoS_2 nanosheets promise to be stable and efficient optical nanoprobes for bioimaging. Herein, strong SHG signals were observed from the CS-MoS_2 nanosheet-treated HeLa cells under 1050 nm fs laser excitation (Figure 4(a)). TPL was observed with 750 nm fs laser (Figure 4(b)), indicating their potential for cell imaging. Furthermore, three-dimensional (3D) imaging of HeLa cells labeled with nanosheets exhibits the shell-like distribution of the TPL, as shown in Figure 4(c), suggesting that the cell membranes are well stained with the nanosheets.

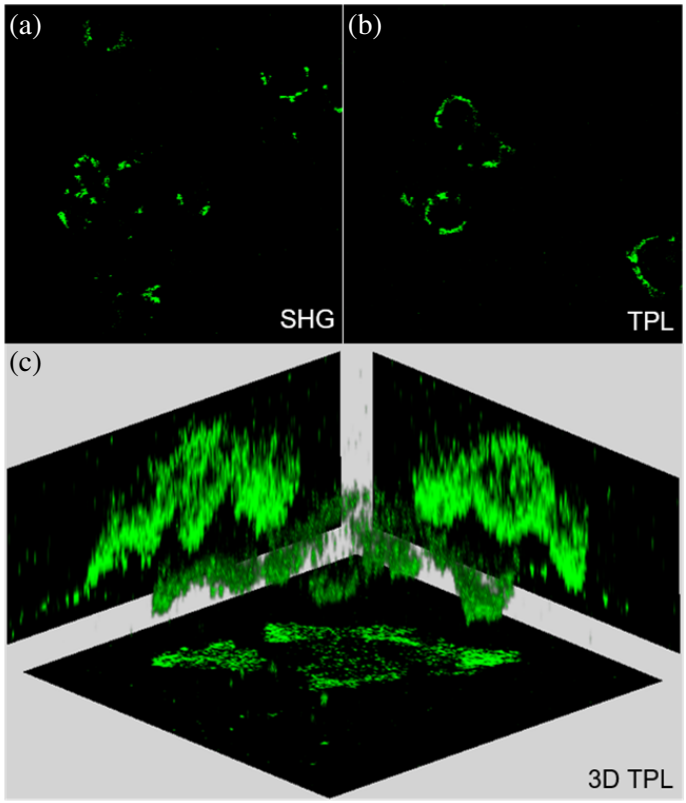

Figure 4. (a) SHG image of CS-MoS_2 nanosheet-treated HeLa cells. (b) TPL image of CS-MoS_2 nanosheet-treated HeLa cells. (c) 3D TPL image of CS-MoS_2 nanosheet-treated HeLa cells by Z-scan.

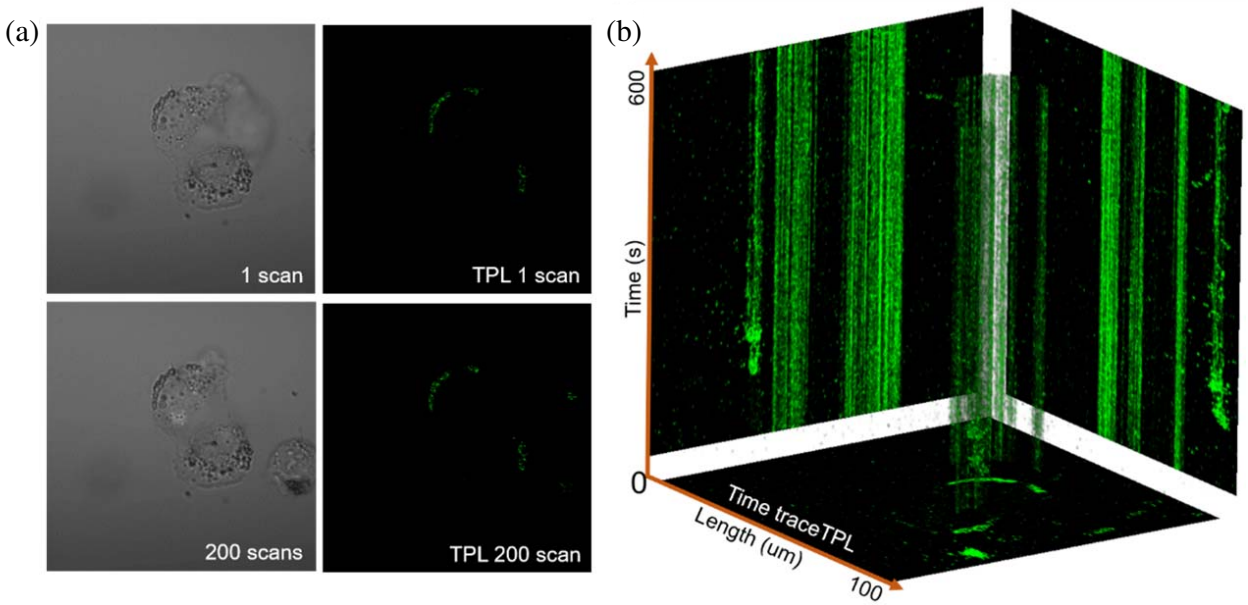

Figure 5. (a) The transmission and TPL images of CS-MoS_2 nanosheets-treated HeLa cells after the addition of methanol during continuous scanning. Each scan consumes $\sim$ 3 seconds. (b) Time trace TPL of CS-MoS_2 nanosheets labeled in HeLa cells under continuous fs laser exposure for an extended time of 600 seconds. The pixel dwell time was 8 µs.

Therefore, CS-MoS_2 nanosheets possess high imaging capability under the first and the second optical imaging window light excitation. As a result, CS-MoS_2 nanosheets reveal good potential for deep bioimaging applications.

Recently, some researchers indicated that the PL of layered MoS_2 nanosheets suffered from quenching on the cellular membrane [12]. The reason for the quenching phenomenon is the transformation of the crystal structure due to the intercalations of alkaline and H^+ ions driven by the so-called membrane potential. However, this was not observed in this case. As shown in Figure 4, TPL from the CS-MoS_2 nanosheet-treated viable cells have not quenched during the scanning process. Figure 5(a) showed the scanning image of CS-MoS_2 nanosheet-treated cells after the addition of methanol. The cells have been nonviable and the intercalations of ions have been disabled. TPL intensities of CS-MoS_2 nanosheets on HeLa cells have hardly any increase between the first and the 200 times scanning images. The time trace TPL image with continuous fs laser exposure for an extend time of 600 seconds also showed hardly any increase in brightness (Figure 5(b)). There is no PL recovery occurred, suggesting that the ions on the cellular membrane have no effect on the TPL of CS-MoS_2 nanosheets. Two potential reasons may be related: (1) the decoration of CS on the surface of MoS_2 nanosheets will not only prevent the direct contact between the nanosheet and cell membrane, but also inhibit the intercalations of ions due to the electrostatic repulsion; (2) those ions cannot affect the PL intensity of single layer MoS_2 nanosheets. Therefore, the non-quenching property of CS-MoS_2 nanosheets improves their potential for bioimaging applications.

4. CONCLUSIONS

In conclusion, the TPL and SHG properties of single layer CS-MoS_2 nanosheets have been systematically studied. Excited by the laser light of first NIR optical window, CS-MoS_2 nanosheets emit strong TPL with a 525 nm band. Under the excitation of the second optical window, CS-MoS_2 nanosheets produce strong SHG. Both the TPL and SHG of CS-MoS_2 nanosheets have shown nonbleaching and nonblinking properties. As a result, CS-MoS_2 nanosheets have been used for TPL, SHG imaging and cellular 3D scanning imaging. Superior to the reported one-photon emission of MoS_2 nanosheets, the TPL of CS-MoS_2 nanosheets has been demonstrated to be non-quenching on the cellular membrane, adding to their advantages in bioimaging applications. The long wavelength NIR excited TPL and SHG from CS-MoS_2 nanosheets using low power also have great potential for deep tissue imaging.

Note

The authors declare that the files (incl. text, figures and data) related to this work leaked out somehow and consequently this work of ours was published by other people in J. Biophotonics in 2018, which has already been retracted after the fact was clarified that this work was originally conducted by Prof. Sailing He and his colleagues at South China Normal University, Guangzhou of China.

ACKNOWLEDGMENT

This research was supported by National Natural Science Foundation of China (NSFC) (61675071, 11974123, 91233208); Program 973 (2014AA014402); Guangdong Provincial Natural Science Fund Projects (2018B030306015, 2019A050510037); the Pearl River Nova Program of Guangzhou (201710010010); the Guangdong Innovative Research Team Program (201001D00104799318).

REFERENCES

1. Novoselov, K. S., A. K. Geim, S. V. Morozov, D. Jiang, Y. Zhang, S. V. Dubonos, I. V. Grigorieva, and A. A. Firsov, "Electric field in atomically thin carbon films," *Science*, Vol. 306, No. 5696, 666–669, 2004, https://doi.org/10.1126/science.1102896.
2. Manzeli, S., D. Ovchinnikov, D. Pasquier, O. V. Yazyev, and A. Kis, "2D transition metal dichalcogenides," *Nat. Rev. Mater.*, Vol. 2, Article number: 17033, 2017, https://doi.org/10.1038/natrevmats.2017.33.

3. Bhimanapati, G. R., Z. Lin, V. Meunier, Y. Jung, J. Cha, S. Das, D. Xiao, Y. Son, M. S. Strano, V. R. Cooper, L. Liang, S. G. Louie, E. Ringe, W. Zhou, S. S. Kim, R. R. Naik, B. G. Sumpter, H. Terrones, F. Xia, Y. Wang, J. Zhu, D. Akinwande, N. Alem, J. A. Schuller, R. E. Schaak, M. Terrones, and J. A. Robinson, "Recent advances in two-dimensional materials beyond graphene," *ACS Nano*, Vol. 9, No. 12, 11509–11539, 2015, https://doi.org/10.1021/acsnano.5b05556.
4. Dong, N., Y. Li, S. Zhang, X. Zhang, and J. Wang, "Optically induced transparency and extinction in dispersed MoS_2, $MoSe_2$, and graphene nanosheets," *Adv. Opt. Mater.*, Vol. 5, No. 19, 1700543, 2017, https://doi.org/10.1002/adom.201700543.
5. Wang, Q. H., K. Kalantar-Zadeh, A. Kis, J. N. Coleman, and M. S. Strano, "Electronics and optoelectronics of two-dimensional transition metal dichalcogenides," *Nat. Nanotechnol.*, Vol. 7, 699–712, 2012, https://doi.org/10.1038/nnano.2012.193.
6. Liu, T., C. Wang, X. Gu, H. Gong, L. Cheng, X. Shi, L. Feng, B. Sun, and Z. Liu, "Drug delivery with PEGylated MoS_2 nano-sheets for combined photothermal and chemotherapy of cancer," *Adv. Mater.*, Vol. 26, No. 21, 3433–3440, 2014, https://doi.org/10.1002/adma.201305256.
7. Gao, W., Y. H. Lee, R. Jiang, J. Wang, T. Liu, and X. Y. Ling, "Localized and continuous tuning of monolayer MoS_2 photoluminescence using a single shape-controlled Ag nanoantenna," *Adv. Mater.*, Vol. 28, No. 4, 701–706, 2016, https://doi.org/10.1002/adma.201503905.
8. Wang, H., B. H. Chen, X. Y. Zhang, S. Liu, B. Q. Zhu, J. Wang, K. Wu, and J. P. Chen, "Ethanol catalytic deposition of MoS_2 on tapered fiber," *Photonics Res.*, Vol. 3, No. 3, A102–A107, 2015, https://doi.org/10.1364/prj.3.00a102.
9. Guan, G., S. Zhang, S. Liu, Y. Cai, M. Low, C. P. Teng, I. Y. Phang, Y. Cheng, K. L. Duei, B. M. Srinivasan, Y. Zheng, Y. W. Zhang, and M. Y. Han, "Protein induces layer-by-layer exfoliation of transition metal dichalcogenides," *J. Am. Chem. Soc.*, Vol. 137, No. 19, 6152–6155, 2015, https://doi.org/10.1021/jacs.5b02780.
10. Pi, Y., Z. Li, D. Xu, J. Liu, Y. Li, F. Zhang, G. Zhang, W. Peng, and X. Fan, "1T-phase MoS_2 nanosheets on TiO_2 nanorod arrays: 3D photoanode with extraordinary catalytic performance," *ACS Sustain. Chem. Eng.*, Vol. 5, No. 6, 5175–5182, 2017, https://doi.org/10.1021/acssuschemeng.7b00518.
11. Mak, K. F., C. Lee, J. Hone, J. Shan, and T. F. Heinz, "Atomically thin MoS_2: A new direct-gap semiconductor," *Phys. Rev. Lett.*, Vol. 105, 136805, 2010, https://doi.org/10.1103/PhysRevLett.105.136805.
12. Ou, J. Z., A. F. Chrimes, Y. Wang, S. Y. Tang, M. S. Strano, and K. Kalantar-Zadeh, "Ion-driven photoluminescence modulation of quasi-two-dimensional MoS_2 nanoflakes for applications in biological systems," *Nano Lett.*, Vol. 14, No. 2, 857–863, 2014, https://doi.org/10.1021/nl4042356.
13. Wang, N., F. Wei, Y. Qi, H. Li, X. Lu, G. Zhao, and Q. Xu, "Synthesis of strongly fluorescent molybdenum disulfide nanosheets for cell-targeted labeling," *ACS Appl. Mater. Interfaces*, Vol. 6, No. 22, 19888–19894, 2014, https://doi.org/10.1021/am505305g.
14. Li, J. L., H. C. Bao, X. L. Hou, L. Sun, X. G. Wang, and M. Gu, "Graphene oxide nanoparticles as a nonbleaching optical probe for two-photon luminescence imaging and cell therapy," *Angew. Chemie — Int. Ed.*, Vol. 51, No. 8, 1830–1834, 2012, https://doi.org/10.1002/anie.201106102.
15. Qian, J., D. Wang, F. H. Cai, W. Xi, L. Peng, Z. F. Zhu, H. He, M. L. Hu, and S. He, "Observation of multiphoton-induced fluorescence from graphene oxide nanoparticles and applications in invivo functional bioimaging," *Angew. Chemie — Int. Ed.*, Vol. 51, No. 42, 10570–10575, 2012, https://doi.org/10.1002/anie.201206107.
16. Zhang, S., N. Dong, N. McEvoy, M. OBrien, S. Winters, N. C. Berner, C. Yim, Y. Li, X. Zhang, Z. Chen, L. Zhang, G. S. Duesberg, and J. Wang, "Direct observation of degenerate two-photon absorption and its saturation in WS_2 and MoS_2 monolayer and few-layer films," *ACS Nano*, Vol. 9, No. 7, 7142–7150, 2015, https://doi.org/10.1021/acsnano.5b03480.
17. Shi, L., L. A. Sordillo, A. Rodríguez-Contreras, and R. Alfano, "Transmission in near-infrared optical windows for deep brain imaging," *J. Biophotonics*, Vol. 9, Nos. 1–2, 38–43, 2016, https://doi.org/10.1002/jbio.201500192.

18. Yin, W., L. Yan, J. Yu, G. Tian, L. Zhou, X. Zheng, X. Zhang, Y. Yong, J. Li, Z. Gu, and Y. Zhao, "High-throughput synthesis of single-layer MoS_2 nanosheets as a near-infrared photothermal-triggered drug delivery for effective cancer therapy," *ACS Nano*, Vol. 8, No. 7, 6922–6933, 2014, https://doi.org/10.1021/nn501647j.
19. Chou, S. S., B. Kaehr, J. Kim, B. M. Foley, M. De, P. E. Hopkins, J. Huang, C. J. Brinker, and V. P. Dravid, "Chemically exfoliated MoS_2 as near-infrared photothermal agents," *Angew. Chemie — Int. Ed.*, Vol. 52, No. 15, 4160–4164, 2013, https://doi.org/10.1002/anie.201209229.
20. Li, Y., N. Dong, S. Zhang, X. Zhang, Y. Feng, K. Wang, L. Zhang, and J. Wang, "Giant two-photon absorption in monolayer MoS_2," *Laser Photonics Rev.*, Vol. 9, No. 4, 427–434, 2015, https://doi.org/10.1002/lpor.201500052.
21. Malard, L. M., T. V. Alencar, A. P. M. Barboza, K. F. Mak, and A. M. De Paula, "Observation of intense second harmonic generation from MoS_2 atomic crystals," *Phys. Rev. B — Condens. Matter Mater. Phys.*, Vol. 87, 201401(R), 2013, https://doi.org/10.1103/PhysRevB.87.201401.
22. Zeng, J., M. Yuan, W. Yuan, Q. Dai, H. Fan, S. Lan, and S. Tie, "Enhanced second harmonic generation of MoS_2 layers on a thin gold film," *Nanoscale*, Vol. 7, No. 32, 13547–13553, 2015, https://doi.org/10.1039/C5NR03133H.
23. Wang, R., H. C. Chien, J. Kumar, N. Kumar, H. Y. Chiu, and H. Zhao, "Third-harmonic generation in ultrathin films of MoS_2," *ACS Appl. Mater. Interfaces*, Vol. 6, No. 1, 314–318, 2014, https://doi.org/10.1021/am4042542.
24. Zhang, W., Y. Wang, D. Zhang, S. Yu, W. Zhu, J. Wang, F. Zheng, S. Wang, and J. Wang, "A one-step approach to the large-scale synthesis of functionalized MoS_2 nanosheets by ionic liquid assisted grinding," *Nanoscale*, Vol. 7, No. 22, 10210–10217, 2015, https://doi.org/10.1039/c5nr02253c.
25. Eda, G., H. Yamaguchi, D. Voiry, T. Fujita, M. Chen, and M. Chhowalla, "Photoluminescence from chemically exfoliated MoS_2," *Nano Lett.*, Vol. 11, No. 12, 5111–5116, 2011, https://doi.org/10.1021/nl201874w.
26. Bao, H., Y. Pan, Y. Ping, N. G. Sahoo, T. Wu, L. Li, J. Li, and L. H. Gan, "Chitosan-functionalized graphene oxide as a nanocarrier for drug and gene delivery," *Small*, Vol. 7, No. 11, 1569–1578, 2011, https://doi.org/10.1002/smll.201100191.
27. Shang, N. G., P. Papakonstantinou, S. Sharma, G. Lubarsky, M. Li, D. W. McNeill, A. J. Quinn, W. Zhou, and R. Blackley, "Controllable selective exfoliation of high-quality graphene nanosheets and nanodots by ionic liquid assisted grinding," *Chem. Commun.*, Vol. 48, No. 13, 1877–1879, 2012, https://doi.org/10.1039/c2cc17185f.
28. Li, H., Q. Zhang, C. C. R. Yap, B. K. Tay, T. H. T. Edwin, A. Olivier, and D. Baillargeat, "From bulk to monolayer MoS_2: Evolution of Raman scattering," *Adv. Funct. Mater.*, Vol. 22, No. 7, 1385–1390, 2012, https://doi.org/10.1002/adfm.201102111.
29. Lee, C., H. Yan, L. E. Brus, T. F. Heinz, J. Hone, and S. Ryu, "Anomalous lattice vibrations of single- and few-layer MoS_2," *ACS Nano*, Vol. 4, No. 5, 2695–2700, 2010, https://doi.org/10.1021/nn1003937.
30. Li, B. L., H. L. Zou, L. Lu, Y. Yang, J. L. Lei, H. Q. Luo, and N. B. Li, "Size-dependent optical absorption of layered MoS_2 and DNA oligonucleotides induced dispersion behavior for label-free detection of single-nucleotide polymorphism," *Adv. Funct. Mater.*, Vol. 25, No. 23, 3541–3550, 2015, https://doi.org/10.1002/adfm.201500180.
31. Splendiani, A., L. Sun, Y. Zhang, T. Li, J. Kim, C. Y. Chim, G. Galli, and F. Wang, "Emerging photoluminescence in monolayer MoS_2," *Nano Lett.*, Vol. 10, No. 4, 1271–1275, 2010, https://doi.org/10.1021/nl903868w.
32. Wang, Y., J. Z. Ou, S. Balendhran, A. F. Chrimes, M. Mortazavi, D. D. Yao, M. R. Field, K. Latham, V. Bansal, J. R. Friend, S. Zhuiykov, N. V. Medhekar, M. S. Strano, and K. Kalantar-Zadeh, "Electrochemical control of photoluminescence in two-dimensional MoS_2 nanoflakes," *ACS Nano*, Vol. 7, No. 11, 10083–10093, 2013, https://doi.org/10.1021/nn4041987.
33. Zhan, Q., J. Qian, H. Liang, G. Somesfalean, D. Wang, S. He, Z. Zhang, and S. Andersson-Engels, "Using 915 nm laser excited $Tm^{3+}/Er^{3+}/Ho3^{3+}$-Doped NaYbF4 upconversion nanoparticles for *in Vitro* and deeper *in Vivo* bioimaging without overheating irradiation," *ACS Nano*, Vol. 5, No. 5,

3744–3757, 2011, https://doi.org/10.1021/nn200110j.

34. Wu, S., G. Han, D. J. Milliron, S. Aloni, V. Altoe, D. V. Talapin, B. E. Cohen, and P. J. Schuck, "Non-blinking and photostable upconverted luminescence from single lanthanide-doped nanocrystals," *Journal Proceedings of the National Academy of Sciences of the United States of America*, Vol. 106, No. 27, 10917–10921, 2014, https://doi.org/10.1073/pnas.0904792106.
35. Wu, R., Q. Zhan, H. Liu, X. Wen, B. Wang, and S. He, "Optical depletion mechanism of upconverting luminescence and its potential for multi-photon STED-like microscopy," *Opt. Express.*, Vol. 23, No. 25, 32401–32412, 2015, https://doi.org/10.1364/OE.23.032401.
36. Zhan, Q., H. Liu, B. Wang, Q. Wu, R. Pu, C. Zhou, B. Huang, X. Peng, H. Ågren, and S. He, "Achieving high-efficiency emission depletion nanoscopy by employing cross relaxation in upconversion nanoparticles," *Nat. Commun.*, Vol. 8, 1–11, 2017. https://doi.org/10.1038/s41467-017-01141-y.